The Eight Classes of Positive-Curvature Graphitic Nanocones

Douglas J. Klein and Alexandru T. Balaban*

Texas A&M University—Galveston, MARS, 5007 Avenue U, Galveston, Texas 77551

Received August 19, 2005

The eight different classes of single-wall positive-curvature graphitic nanocones are emphasized, characterized, and illustrated. Local transformations among different possible apex-region structures within a common class are investigated, it being noted that there is no short sequence of such transformations which convert from any one of these eight classes to another. Attention is directed to class identification and to nanocone codes, especially for "buckycones" comprised solely from pentagonal and hexagonal rings.

INTRODUCTION

Almost all of the several dozens of publications on single-wall graphene nanocones (SWNCs) mention five types of "standard" nanocones which may be obtained by mutually attaching the dangling bonds of a number q of 60° sectors of graphene, where $q = 1$, 2, 3, 4, or 5. See, for example, refs 1 and 2 or Ebbesen's review,[3] which is rich in experimental data. Thus, Figure 1 presents the formation of a nanocone with a pentagon at the apex by deleting one 60° sector of a graphene sheet. However, the mutual compensation of the dangling bonds might also be made in a skewed fashion, for example, by connecting 1 to 2′, 2 to 3′, and so forth, with the bond at 1′ left dangling or the atom 1′ could be deleted with the two then-formed dangling bonds connected together. Or one could entertain connecting i to $i' + 2$, and so forth, and such different manners of reconnection could be considered for different numbers q of sectors. Indeed, one could entertain making such decalated reconnections even in the case of $q = 6$ sectors (though these are cones degenerated to the "flat" circumstance). But, in fact, it is known what happens in such a decalation, namely, there result *dislocations* of different Burgers vectors; see Burgers[4] or many other works, for example, refs 5−7. And each such dislocation is as different from graphite as are the five standard nanocones—in that to construct any one of these (dislocation or SWNC) from graphite entails cutting and reattaching comparable numbers of bonds ($\sim N$ bonds in an $\sim N \times N$ graphene sheet).

Thence, it is natural to investigate the effect of decalation on cones or, equivalently, the effect of surrounding different defect regions by a planar locally graphitic sea of hexagons, and this we do here. Indeed it is emphasized that, as the result of such decalation, there result more than five classes of positive-curvature graphitic nanocones, though there are still just five apex angles. Here, this is emphasized and different simplified means by which to determine in which class a nanocone belongs are established. Also, a more refined naming of individual SWNCs is developed, particularly for the special SWNCs (so-called "buckycones") with degree-3 vertexes and all rings either hexagonal or pentagonal. Thereafter, we illustrate numerous examples of finite (local) transformations (or reactions) leading from one SWNC to another, while at the same time the overall nanocone class is conserved. Finally, some overall discussion follows, with the introduction of some summary nanocone characteristics.

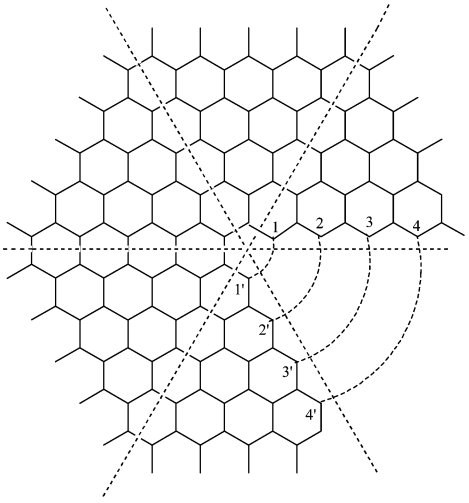

Figure 1. Formation of a graphene nanocone with a pentagon at the apex from $q = 5$ sectors.

NANOCONES

Evidently, by deleting one through five 60° sectors, one obtains five stepwise decreasing apical angles, independent of the (fixed finite) decalation of the reconnection. One can define the consequent apical angles (after assimilating the network to a circular cone) either as solid angles occluded by the cone and measured in steradians or more simply as linear angles α formed by the intersection of (the unstretched but slightly bent graphene sheets of) the cone with a plane containing the cone axis.

Table 1 presents the first seven choices for sector numbers of graphene nets, encompassing the positive-curvature SWNCs, along with the "degenerate" cases of nanotubes at $q = 0$ and "flat" graphene networks at $q = 6$. The associated apical angles α are also given. The net Gaussian curvature of the apex region is denoted by κ and is given by

$$\kappa = \pi(6 - q)/3 \quad (1)$$

* Corresponding author e-mail: balabana@tamug.edu.

10.1021/ci0503356 CCC: $33.50
Published on Web 11/09/2005

Table 1. Data for the First Seven Numbers of Sectors

sectors q	α (deg)	σ (srad)	κ (srad)	Q (radians)	disclinations p	nanocone or congener
0	0.0	0	2π	0	6	nanotube (SWNT) + cap
1	19.2	0.087	$5\pi/3$	$\pi/3$	5	first (sharp) SWNC
2	38.9	0.36	$4\pi/3$	$2\pi/3$	4	second SWNC
3	60.0	0.84	π	π	3	third SWNC
4	83.6	1.60	$2\pi/3$	$4\pi/3$	2	fourth SWNC
5	112.9	2.81	$\pi/3$	$5\pi/3$	1	fifth (blunt) SWNC
6	180.0	6.28	0	2π	0	graphene

Table 2. The Eight Classes of Nanocones

disclinations, p	sectors, q	$\mathscr{M}$	class	**m**	criteria
5	1	1	5,1	**0**	none
4	2	1	4,1	**0**	$x_2 - x_1 = 3k$
		2	4,2	$\mathbf{e_2}$	$x_2 - x_1 \neq 3k$
3	3	1	3,1	**0**	$\mathrm{mod}_2x_1 + \mathrm{mod}_2x_2 + \mathrm{mod}_2x_3 = 3k$
		3	3,3	$\mathbf{e_3}$	$\mathrm{mod}_2x_1 + \mathrm{mod}_2x_2 + \mathrm{mod}_2x_3 \neq 3k$
2	4	1	2,1	**0**	$\lvert x_1 - x_2 + x_3 - x_4\rvert = 3k$
		2	2,2	$\mathbf{e_4}$	$\lvert x_1 - x_2 + x_3 - x_4\rvert \neq 3k$
1	5	1	5,1	**0**	none

Also given in Table 1 is the planar angle $Q = q \times 60°$ formed by the q sectors, as well as the net solid angle σ occluded by the cone when viewed from a position external to the nanocone. The disclination number p, which is just $6 - q$, also presented in Table 1, is proportional to κ. Notably, for the case when the faces are solely pentagons and hexagons and all vertexes have a degree of 3, p is also the number of pentagons. Two pentagons are equivalent to one square or to a (heteroatomic) vertex of degree 2, and three pentagons are equivalent to a triangle (while retaining all vertexes of degree 3). Such equivalences are in consonance with Euleric formulas for embeddings of networks in finite boundary-less surfaces S:

$$\Sigma_i n_i(6 - i) + 2\Sigma_d \upsilon_d(3 - d) = 6\chi_S \text{ or}$$

$$3n_3 + 2n_4 + n_5 + 0n_6 - n_7 - 2n_8 \ldots + 2\upsilon_2 + 0\upsilon_3 - 2\upsilon_4 - 4\upsilon_5 - \ldots = 6\chi_S \quad (2)$$

where n_i is the number of i-membered rings in the network, υ_d is the number of vertexes of degree d, and χ_S is the Euler-Poincaré characteristic for the surface S, with $\chi_S = 2$ for a surface S equivalent to a sphere (as for polyhedra), $\chi_S = 0$ for a torus, or generally $\chi_S = 2 - 2g$ for an orientable surface S of genus g. The number n_6 of benzenoid rings and the number υ_3 of vertexes of degree 3 (such as sp^2-hybridized carbon atoms) appear in eq 2 with zero coefficients, so that this relation does not limit their variation. If 12 pentagons are needed to close a polyhedron containing only pentagons and hexagons, this means that each pentagon contributes a disclination of $720°/12 = 60°$, which then also is the associated net Gaussian curvature. A square or two pentagons would contribute with 120°, a triangle or three pentagons with 180°, and a heptagon with an opposite disclination (−60°). Such negative curvatures lead to fluted or crenellated saddle-shaped geometries and are not common in nanocones because they would involve more than six 60° graphene sectors. Overall, the various chemically relevant equivalences may be summarized as follows:

$$\begin{aligned}
\text{2-gon (or lune)} &\approx 4 \text{ pentagons}\\
\text{3-gon (or triangle)} &\approx 3 \text{ pentagons}\\
\text{4-gon (or square)} &\approx 2 \text{ pentagons} \approx \text{degree-2 vertex}\\
\text{7-gon} &\approx -1 \text{ pentagon}\\
\text{8-gon} &\approx -2 \text{ pentagons} \approx \text{degree-4 vertex}\\
\text{9-gon} &\approx -3 \text{ pentagons}
\end{aligned} \quad (3)$$

Here, the case of a 5-gon is omitted as it is the choice for the unit of measure of Gaussian curvature. Also, neither the 6-gon nor the degree-3 vertex appear since they form the "flat" background frame against which the curvature is measured.

In concise summary, we have

$$p = \sum_{i\geq 2}(6 - i)n_i + 2\sum_d (3 - d)\upsilon_d \quad (4)$$

The difference between eqs 2 and 4 is that eq 2 is for a closed finite surface S, whereas eq 4 is for the circumstance of an infinitely extended planar network. It may also be noted that, upon multiplication by $2\pi/3$, the right-hand side of eq 4 gives the various so-called "local combinatorial curvatures",[8,9] while the left-hand side gives the net Gaussian curvature κ. A similar multiplication of eq 2 by $2\pi/3$ gives the net Gaussian curvature of S expressed in terms of local contributions.

For a circular nanocone of type p, the apical angle is

$$\alpha = 2\arcsin(Q/2\pi) \quad (5)$$

and the solid angle is

$$\sigma = 2\pi[1 - \cos(\alpha/2)] = 2\pi - (4\pi^2 - Q^2)^{1/2} \quad (6)$$

The disclination number p is the number of pentagons at the apex region (if all defecting is due to pentagons, as for "buckycones"). Beyond the five SWNC cases with $q = 1$, 2, 3, 4, and 5 graphene sectors, Table 1 contains two extreme cases: (i) the plane graphene sheet, which can be considered as a nanocone with $q = 6$ sectors (with $\alpha = \pi$ and $Q = 2\pi$), and (ii) a single-wall carbon nanotube capped at one end,

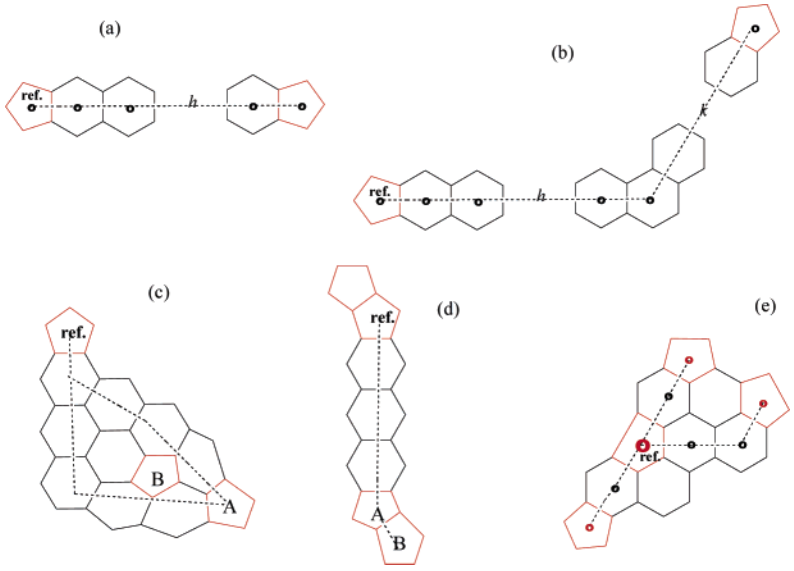

Figure 2. (a) An interpentagon path [*h*,0] along an acenic string of hexagons. (b) A normal [*h*,*k*] path. (c) An illustration of the two single paths from the reference pentagon to A. (d) Paths from the reference pentagon are [4,0] for A and [4,1] for B. (e) Canonical notation for interpentagon paths and consequent nanocone code: [20:2:20:2:21].

which can be considered as a nanocone with apical divergence angle $\alpha = 0$ and without even a single sector (so, $q = 0$). A common cap for nanotubes with six isolated pentagons obtained experimentally is half of buckminsterfullerene. Experimentally, nanoconic structures of some sort have been observed, starting with Gillot et al. in 1968[10] and others,[11−13] and the SWNCs considered here became firmly established with Sattler and co-workers.[14−16] Now (as reviewed by Ebbesen[3]), all five angles of cones have been detected. The $q = \alpha = 0$ case of buckytubes is even more widely seen and studied.

Various kinds of local apical defects in a graphene sheet giving rise to five values of positive curvature for SWNCs have been considered,[1,2,17,18] and a close degree of correspondence to the earlier[12] "helical cones" applies. But, by analyzing the topology and geometry of nanocones, it was proved[19] that there are eight classes of positive-curvature SWNCs, which for infinitely extended nanocones cannot be changed into one another through a finite number of changes (and a similar result[20] applies for square-planar lattice cones). These eight "circum-matching" classes occur because the three cases with $q = 2$, 3, and 4 each give rise to two SWNC classes, as indicated in Table 2.

The basis of this classification[19] consists of the circumambulatory paths formed of strips of hexagons surrounding the "local defect" of the polygons forming the apex of the SWNC. Henceforth, these are called *circumpaths*, it being understood that these paths are made out of linear ("acenic") strips of hexagons around the local defect with turns at 120°. Then, for a given type of cone, there are q such acenic portions, whose successive lengths $(x_1, x_2, ..., x_q) \equiv \mathbf{x}$ characterize the circumpath. The criteria differentiating pairs of classes with $q = 2$, 3, and 4 are indicated in Table 2, the eight classes of SWNCs being denoted as "Class $p,\mathscr{M}$". These pairs have different so-called *quasi-spin* values $S = 0$, $^1/_2$, or 1, which is such that the quasi-spin multiplicity $\mathscr{M} = 2S + 1$ identifies the number of subclasses into which each SWNC class may be resolved if rotations about the cone axis are disallowed. This further resolution becomes relevant if the SWNC's orientation about its cone axis is somehow fixed, say, as relative to another adjacent SWNC in a multiwall nanocone. But, we do not consider this further here, though we use the multiplicity $\mathscr{M}$ to label the different SWNC classes. The vectorial label **m** is discussed in refs 19 and 20 and also in Appendix A, where the results of the last column of Table 2 are derived. These criteria on **x** are conveniently used to distinguish the eight SWNC classes. Indeed, these criteria are shown in Appendix A to distinguish further classes of negative curvatures.

To date, experimental data seem to have been focused on a scale such that, though α is observed, the finer scale of atomic interconnections which would determine the class has not been reached. Nevertheless, it is emphasized that, with the species in different classes being related only through an infinite sequence of finite changes, some properties should be correspondingly different, even qualitatively different.

BUCKYCONES AND CODES

The special cases with all degree-3 vertexes and the only nonhexagonal rings being pentagons are of special interest and are here termed *fullerenic nanocones* or, more briefly, *buckycones*. Here, we seek a general labeling for these nanocones (many of which belong to the same overall nanocone class when they have the same numbers p of pentagons). Basically, we simply specify canonical paths between various pairs of pentagons. Such a canonical shortest path steps from a pentagon ring center to an adjacent ring center with the steps insofar as possible through opposite sides of intervening hexagons through which the walk passes. Sometimes, one may traverse from one pentagon to another with all successive pairs of steps through opposite sides of all the h intervening hexagons in an acenic strip, as in Figure 2a. In other cases, a bend or turn must be made, as in Figure 2b, with the turn, by convention, always being taken through 120° and to the "left", when one views the buckycone from the "outside". Such a path is then specified by the numbers h and k of steps in the two "straight" sections through hexagons. In the case of Figure 2a, it is understood that the length $k = 0$, and the *canonical path* notation will be [h,0],

not [0,*h*]. Two adjacent pentagons give rise to the notation [1,0] for the corresponding walk. If there are two [*h*,*k*] paths from a reference pentagon, as in Figure 2c, then the one with the lexicographically first [*h*,*k*] designation is taken as the canonical code. Thence, in Figure 2c, the canonical code is [1,4], rather than [3,3]. In yet other cases, a walk between two pentagons must either pass through a pentagon or else make two turns. Such a case is indicated in Figure 2d, where the indicated [4,1] path makes its turn at a pentagon. We retain the convention of a single turn to the left for any path between two pentagons but allow the possibility that the turn may be made at a pentagon. That is, a turn occurs whenever the walk enters through one side and exits through the next-neighbor side to the left; there is no turn if the exit is made through the next-next-neighbor side (both to the left and to the right). In specifying the different paths from a reference pentagon, if there are two paths [*h*,0] and [*h*,*k*] with the *h* steps along the same direction, then it is evident that the [*h*,*k*] path makes its turn at a pentagon (and, otherwise, all intervening steps are at hexagons).

A *p*-pentagon buckycone, then, is to be designated by the set of $p - 1$ canonical interpentagon paths from a given reference pentagon if one further designates the relative directions these paths take from the reference pentagon. Thence, granted the reference pentagon, the buckycones may be so designated unambiguously. The code for a buckycone with *p* pentagons will be

$$[h_{12}k_{12}{:}t_{2(1)3}{:}h_{13}k_{13}{:}\ldots{:}t_{p-1(1)p}{:}h_{1p}k_{1p}]$$

where the reference pentagon is assigned number 1, with h_{ij},k_{ij} the canonical path from pentagon *i* to pentagon *j*, and the angle (to the left) between two successive canonical paths from *i* to *j* and from *i* to *k* is $t_{j(i)k} \times 72°$. An example is given in Figure 2e for the case of $p = 4$ pentagons. (If two digits are needed to specify h_{ij} or k_{ij}, one inserts commas between h_{ij} and k_{ij}). A choice of the reference pentagon needs to be made, it seeming that a choice of a relatively more central location for reference should facilitate fewer occurrences with overlapping, multiple, or otherwise complicated paths from the reference to each other pentagon. This "centrality" goal is made explicit by choosing the reference pentagon numbered 1 to be such that the distance sum $s_1 \equiv \sum_i^{\neq 1}(h_{1i} + k_{1i})$ is a minimum. {From such a reference pentagon 1, the [h_{1i}, k_{1i}] paths should be well-defined (along with s_1), though for some (presumably less centrally located) pentagons, it might sometimes happen that the [*h*,*k*] paths to all other pentagons are not defined as simply as we wish. For a general pentagon (*j*), one can unambiguously define $s_j \equiv \sum_i^{\neq j} d_{ij}$ with the sum over degree-5 sites in the dual lattice with d_{ij} being the shortest-path distance between sites *i* and *j*. Again, the minimum s_{ij} is chosen to identify the reference, taken as $j = 1$, in which case, the [*h*,*k*] path is more likely to be nicely defined. Indeed, such is the case for all the examples we have examined}. If two or more pentagons realize the minimum, a choice of the lexicographically first is made. This is illustrated in the next section.

This notation for buckycones can even be extended to deal with some more general SWNCs, allowing rings of sizes other than five and six but (most conveniently) still retaining the condition that all vertexes are of degree 3. Such 3-regular planar networks with an infinite number of hexagonal faces we term *cubic nanocones*. (One conceivable convention would be that an interpentagon path $h = k = 0$ designates a square ring, leading to a canonical notation [0,0], and two interpentagon 0-distances from the reference pentagon could designate a triangular ring). But, we prefer simply to use the symbol of the preceding paragraph to locate different defect rings, with an added notation to indicate the size of the ring so located. This added notation is simply the ring's size enclosed in parentheses with the understanding that, for pentagons, the parenthetic notation may be suppressed. If two codes (before the addition of the parenthetic designation of the ring sizes) are the same, then that with the lexicographically earlier set of ring sizes is chosen as the preferred code. Thus, [(4)] indicates a $p = 2$ nanocone with a single square at the apex, [(4)10] indicates a pentagon with an adjacent square, and [(4)10(4)] indicates two adjacent squares. Further, a triangle and a digon (lune) can be indicated as [(3)] and [(2)], respectively. In the preceding paragraph, we have taken a convention for what happens when a canonical path passes through hexagons or pentagons along the way, and more generally, we seek to avoid such a path passing through a polygon of another size except at the end points.

A yet further extension is conceivable to allow for different degree vertexes. A degree-2 vertex might be viewed as a lune with its size contracted to 0, so that only a single vertex remains. Likewise, a degree-4 vertex would be square contracted to 0. Thence, we denote these two circumstances by $(2)_0$ and $(4)_0$, respectively. Thus, for example, a degree-2 vertex with all rings being of six atoms is denoted $[(2)_0]$ and is equivalent (in curvature) to two pentagons, as noted in the preceding section, but readily seen when one deletes the degree-2 vertex (•) in the substructure >•—•—•<, resulting in a single bond between the two adjacent degree-3 vertexes (thereby leaving two pentagons). Of course, such different degree sites generally only occur as heteroatoms, so that some further chemical designation generally would be desired to be supplied.

NANOCONE CLASSES ILLUSTRATED

The graphene sheet, which can be considered as "the bluntest cone", has $q = 6$ sectors with an "apical angle α" of π radians $= 180°$ and a solid angle σ corresponding to the ratio between the area of a hemisphere and the square of its radius, $\sigma = 2\pi$ steradians. Here (for $q = 6$), there are an infinite number of classes, each corresponding to a different Burgers vector, as described in many texts, for example, refs 5−7. Similarly, the sharpest case of $q = 0$ has $\alpha = 0$ and an infinite number of classes. These $q = 0$ and $q = 6$ cases are not further considered here, and we go on to the positive-curvature SWNCs with $q = 5$, 4, 3, 2, and 1. In the following figures for these nanocones, we illustrate just the apex region, it being understood that the nanocone extends much further, though solely with graphitically interconnected hexagonal rings.

To summarize, we denote circumpaths **x** by vectorial sequences of acenic segment lengths, separated by commas and enclosed in parentheses; classes by the disclination number *p* separated by a comma from the "quasi-spin multiplicity" $\mathscr{M}$, without brackets; and codes by ring sizes, *hk* acenic-segmented paths, and intervening turn numbers *t*

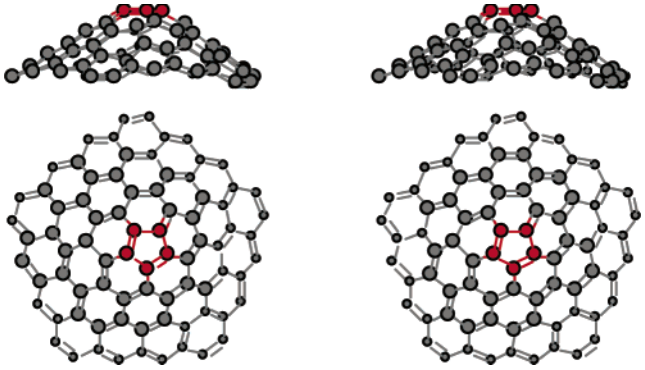

Figure 3. Stereoviews of the unique buckycone of class 1,1 in side and front views.

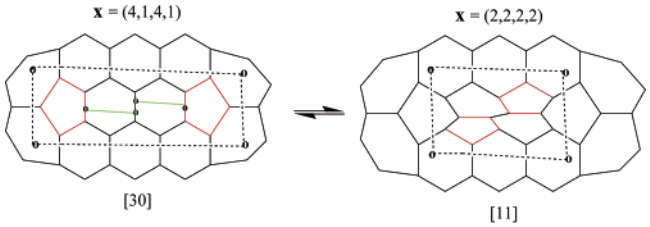

Figure 4. Conversion of a nanocone apex region with two pentagons connected by a shortest path (blue) corresponding to four C−C bonds into another belonging also to class 2,2 and having a shortest path corresponding to a single C−C bond. The green lines denote two C_2 added fragments. The dashed lines are representative circumambulatory circuits $\mathbf{x} = (x_1, x_2, x_3, x_4)$. Buckycone codes before and after the conversion are [30] and [11], respectively.

(between paths), with colons separating paths and turns and all enclosed in square brackets.

One Disclination: Class 1,1 Nanocone. Here (assuming that all vertexes have a degree of 3 and all rings are either pentagons or hexagons), we have the unique buckycone with one pentagon at its apex, illustrated in stereoview in Figure 3. In consonance with the coding of the preceding section, we denote this by [(5)]. Of course, there are also other particular nanocones possible in this class, with the same solid angle, say, with one heptagonal ring and two pentagonal rings or a square and two heptagons, with various possibilities of their relative positions or various possibilities with different degree vertexes.

Two Disclinations: Class 2,1 and 2,2 Nanocones. For this disclination number, the SWNCs fall into two classes (each of which has the same apical angle α and solid angle σ). They can have, at the apex, two pentagons, a square, or a vertex of degree 2 (among other possibilities). When such SWNCs have two pentagons at the apex, the two canonical paths from 1 to 2 and from 2 to 1 are (h_{12},k_{12}) and (h_{21},k_{21}) with $h_{21} = h_{12}$ and $k_{21} = k_{12}$. These buckycones are neatly identified to class 2,1 or 2,2 as the difference $h_{12} - k_{12}$ is or is not a multiple of 3, as shown in Appendix B.

The circumpaths may be chosen to have four acenic portions of successive lengths x_1, x_2, x_1, and x_2. These numbers, separated by commas, can identify a given SWNC class, though of course, there are many such circumpaths for one SWNC. One such (smaller) circumpath designation **x** is shown in Figure 4 above each apex region. The particular apical structures for the example buckycones are labeled by codes, as given below each structure.

Within the same class, by adding or deleting vertexes and edges in the molecular graph, one can convert SWNCs into

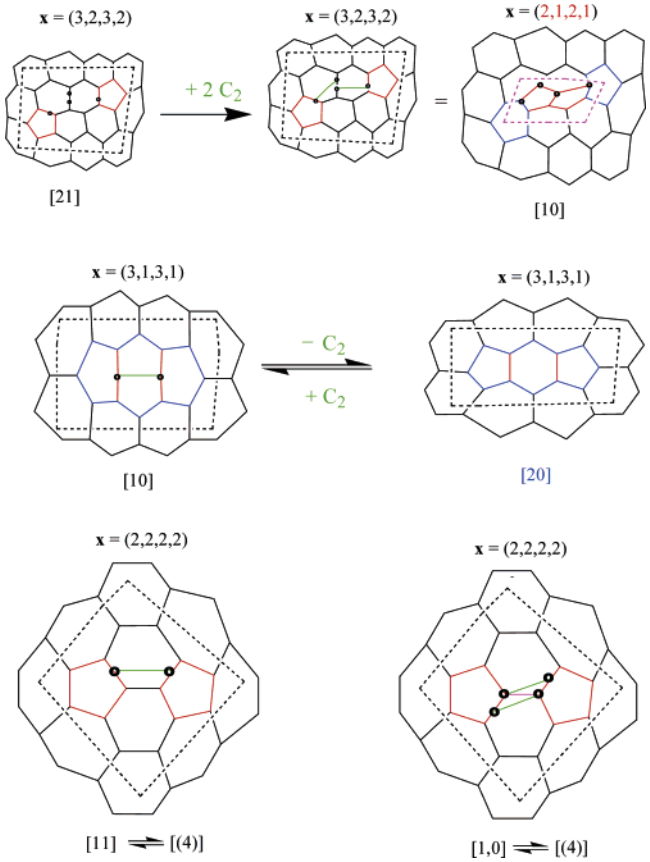

Figure 5. Interconversions within the same class. Top row: conversion of an apex with two pentagons sharing an edge (class 2,2) into an apex with a pair of pentagons connected by a path of length 3. Middle row: conversion of an apex with two pentagons sharing an edge into an apex with two pentagons connected by paths of length 2 (again, class 2,2). Bottom row: two ways for the conversion of an apex with two pentagons connected by a path of length 1 into an apex with a square (class 2,1). Dashed lines identify circumpaths.

one another, but it is not possible to finitely convert class 2,1 nanocones into class 2,2, or vice versa. In Figures 4 and 5, one can see the results of such class-preserving interconversions illustrated with dotted lines for the circumpaths and with a red color indicating pentagons that become blue hexagons by adding one vertex. Green edges (C_2 lines) can be added or deleted. The circumpath of hexagons in acenic portions of the circumpaths are indicated in the same color as the corresponding dotted line. If one were to add one vertex on the green edge in the middle row of the SWNCs with the circumpath label $\mathbf{x} = (3,1,3,1)$, one retains a class 2,2 SWNC, now $[(2)_0]$ with an all-hexagon apex having a vertex of degree 2.

Examples of nanocones belonging to classes 2,1 and 2,2 are presented in Figures 6 and 7, respectively. It was mentioned above that two pentagons are equivalent to one heptagon and three pentagons, or one square, or a vertex of degree 2. In Figures 6 and 8, one sees nanocones manifesting these equivalences.

Three Disclinations: Class 3,1 and 3,3 Nanocones. Next, we examine three-sector nanocones. If, for a buckycone, the three pentagons are equivalently inter-related, then the circumpaths $\mathbf{x} = (x_1, x_2, x_3)$ end up with each component equal ($x_1 = x_2 = x_3$), so that these all belong to class $(p,\mathcal{M}) = (3,1)$. This includes the apex with three mutually abutting

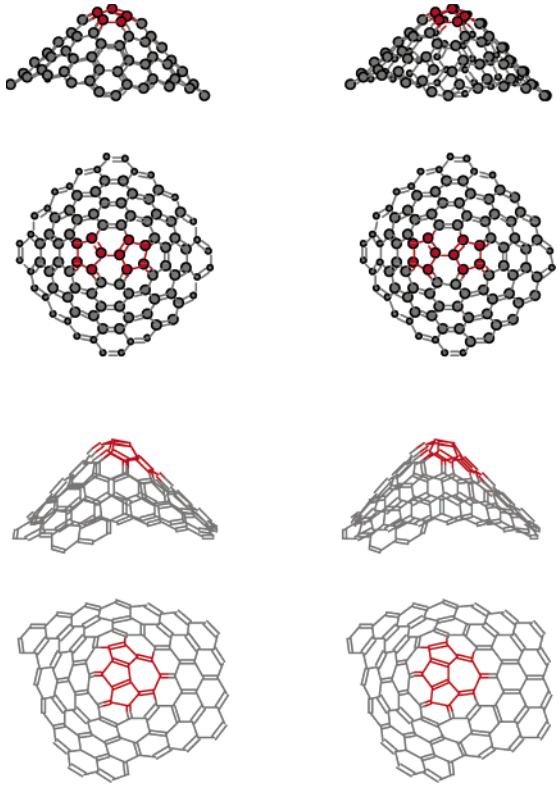

Figure 6. Side and front views of class 2,1 nanocones: (top two lines) [11] with two pentagons, and (bottom two lines) [10:1:10-(7):1:10] with one heptagon and three pentagons.

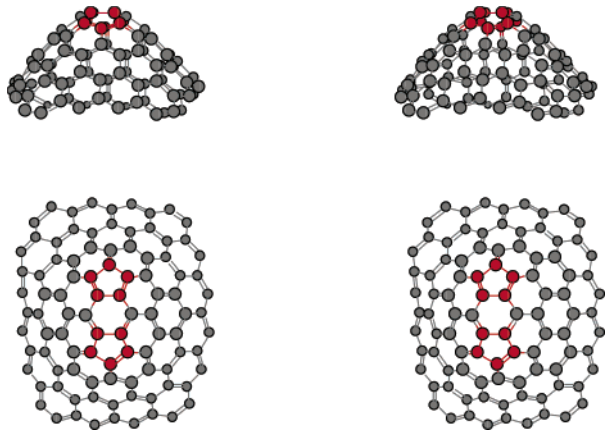

Figure 7. Class 2,2 buckycone [20] (side and front views).

pentagons [10:1:10] and the apex with three pentagons each separated from one another by a single hexagon, [20:1:20]. Both of these and others of the same class, along with possible interconversions with other nanocones in this same class, are indicated in Figures 9 and 10. A circumpath **x** with three components is shown above the apex picture. The nonhexagon sizes and their mode of "linking" (i.e., the nanocone code) are shown in square brackets below the structures. As in Figure 4, the pentagons are shown in red and added lines for interconversions are in green.

The second $p = 3$ class can be realized in different ways. As shown in Appendix C for the cubic nanocones [(4)*hk*] comprised from a square and a pentagon, such a cone is in class 3,1 if both *h* and *k* are even, and otherwise, the cone is in class 3,3. Buckycones can also be in class 3,3, though the three pentagons are not equivalently related.

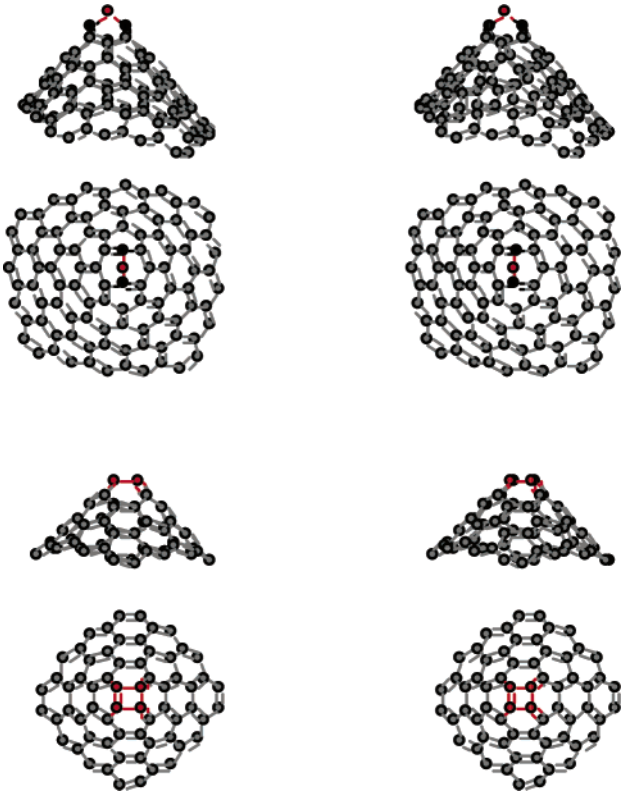

Figure 8. Nanocone (class 2,2) with a vertex of degree 2 which could be represented by a $-CH_2-$ or $-O-$ group (side and front views) and a code $[(2)_0]$ is shown in the first two lines. The next lines show a nanocone (class 2,1) with a square at the apex (side and front views) and code [(4)].

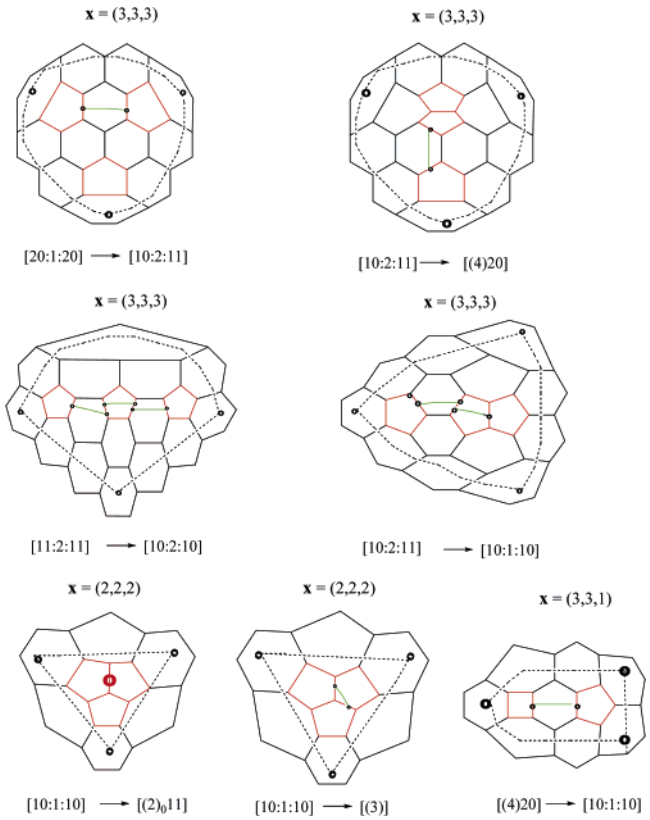

Figure 9. Views of nanocone apexes with three pentagons or (fewer) smaller polygons, along with three-component circumpaths. All are cones of class $(p, \mathcal{M}) = (3,1)$.

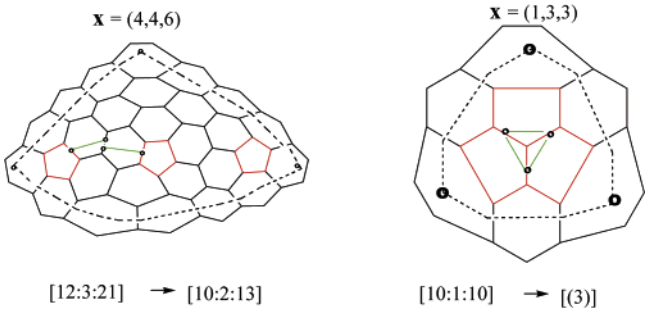

Figure 10. Further examples of class $(p,\mathcal{M}) = (3,1)$ nanocones with interconversions.

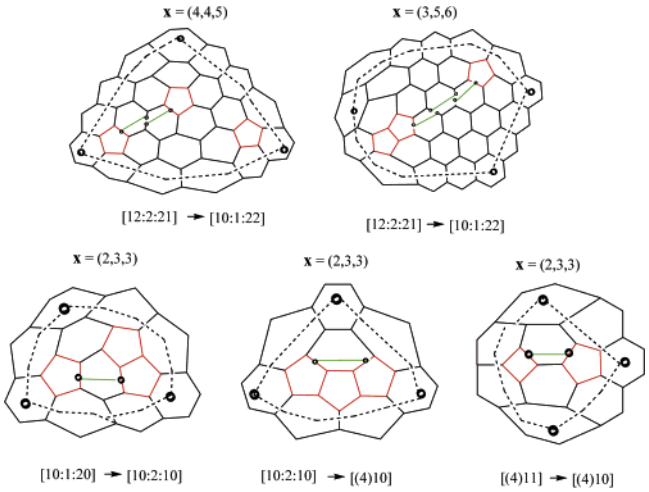

Figure 11. Class $(p,\mathcal{M}) = (3,3)$ nanocones with interconversions.

We present in Figure 11 similar interconversions for class $(p,\mathcal{M}) = (3,3)$ nanocones. In this class, the circumpaths $\mathbf{x} = (x_1, x_2, x_3)$ have one component x_i of a different parity than the other two components, and this circumstance is not changed by any finite sequence of finite reactions (so long as the cone extends infinitely).

A few three-pentagon buckycones from Figures 8 and 9 are presented as stereoviews in Figures 12 and 13. In Figure 14, stereoviews of some cubic nanocones with smaller-sized rings are shown. Particularly, the third of these [(4)20] shows some "polyhedralization" of the nanocone structure, but presumably, this would wash out with a sufficiently larger cone (with a greater number of hexagons around the apex region).

Four Disclinations: Class 4,1 and 4,2 Nanocones. These are globally composed from two sectors, with some local rearrangements, deletions, or additions in the apex region. These cones can have four pentagons, two squares, a square with two pentagons, a triangle with a pentagon, or a lune (or digon), as seen in Figures 14 and 15. In all these cases (or even further cases with different degree vertexes), the circumpath $\mathbf{x} = (x_1, x_2)$ has two components, and whether a nanocone is of class 4,1 or 4,2 corresponds to whether the difference $x_2 - x_1$ is or is not a multiple of 3.

An especially simple ("circumpath-free") determination of the class (4,1 or 4,2) applies if a cubic $p = 4$ nanocone has but two defect rings, such as is reminiscent of the case for $p = 2$ and $p = 3$, all as shown in Appendix C. It turns out that all of those with two squares {i.e., with codes [(4)*hk*(4)]} are in class 4,1. For the [(3)*hk*] nanocones with a triangle and a pentagon, the cone is in class 3,1 or 3,3, according to whether $|h - k|$ is or is not divisible by 3.

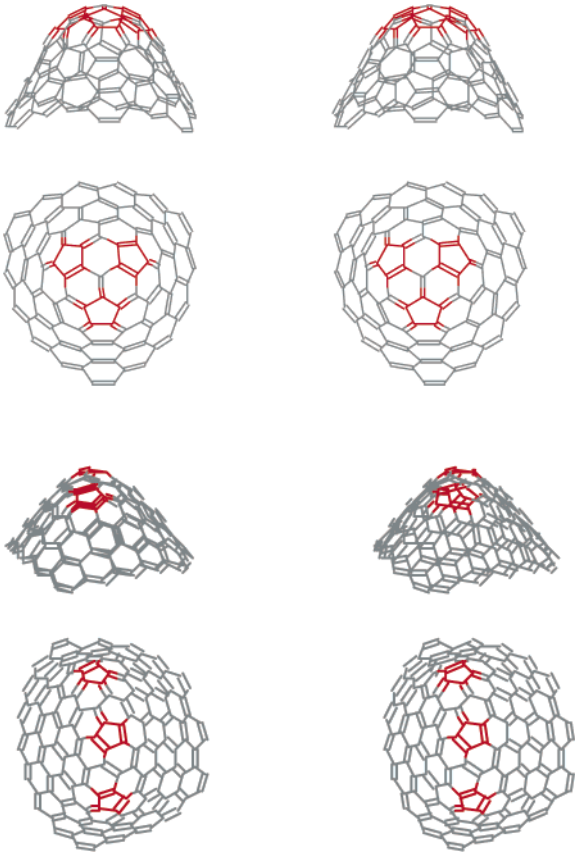

Figure 12. Lateral and frontal stereoviews of class 3,1 nanocones with three pentagons at the apex: [20:1:20] and [12:3:21].

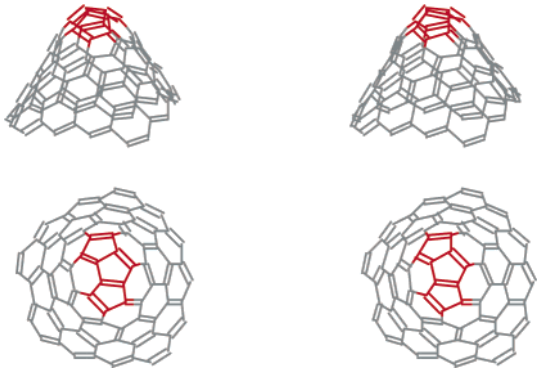

Figure 13. Lateral and frontal stereoviews of a class 3,3 nanocone [10:2:10] with three pentagons at the apex.

A structure with a lune is equivalent to the following bond sequence >•—•═•—•<, where all vertexes have a degree of 3. And this evidently is equivalent to the structure with these two center vertexes deleted and the remaining dangling bonds joined, leaving the two adjacent polygon faces each with two fewer sides, so that (as in eq 3) the lune is seen to be equivalent to four disclinations. Or, alternatively, the two center vertexes could be deleted along with all the bonds incident to them to leave two degree-2 vertexes (which are, again, equivalent to four disclinations).

Further examples of class 4,1 and 4,2 nanocone pentagon apex combinations are presented in Figures 16 and 17, respectively. The arrangement with a lune or two degree-2 vertexes appears in the lower right example of Figure 16.

Stereoviews of class 4,1 buckycones with four pentagons at the apex are shown in Figure 18, and those of class 4,1

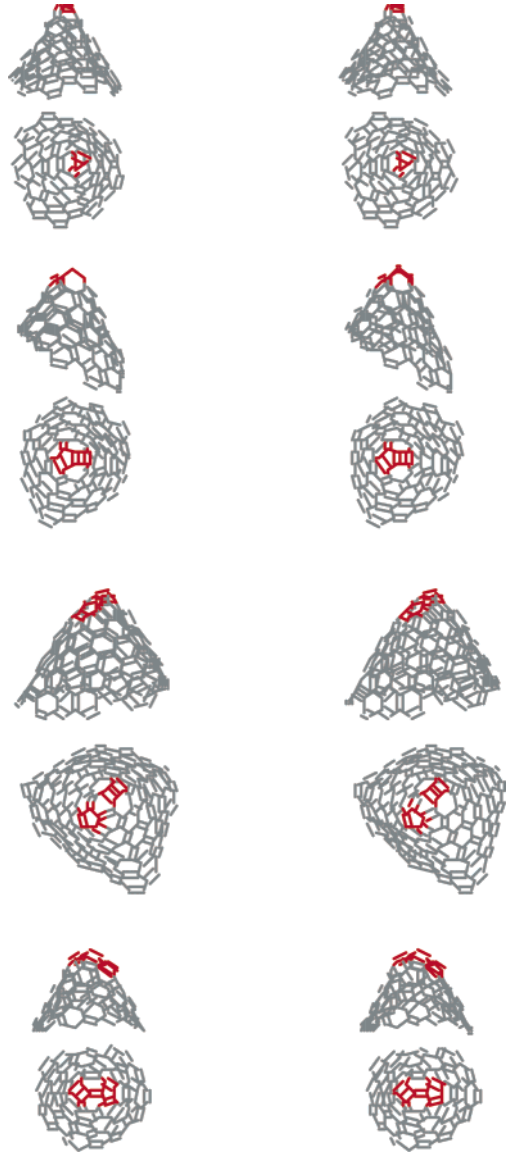

Figure 14. Nanocones in side and front stereoviews. From top to bottom: [(3)], [(4)10], [(4)20], and [(4)21].

nanocones with two squares are shown in Figure 19. (Again, all nanocones [(4)*hk*(4)] are of class 4,1.)

In Figure 20, side and front stereoviews of a class 4,2 buckycone with four pentagons are presented.

Five Disclinations: Class 5,1 Nanocones. With $p = 5$, there again is a single class, which gives rise to the sharpest standard SWNCs, each composable from just a single sector. Many distinct structures are possible, either with variously positioned pentagons, with polygons of smaller size (four-, three-, or two-membered), with vertex degrees different from 3, or finally with a combination of such variations, but all such that, in apex drawings for this curvature (and p value), one has a single-segment circumpath $\mathbf{x} = (x_1)$, as seen in Figure 21.

Figures 22 and 23 present stereoviews for four examples of class 5,1 SWNCs with five pentagons at the apex in the side and front views, respectively. Figure 24 shows a class 5,1 nanocone with a pentagon and a lune at the apex.

DISCUSSION

There are a few additional points which may be made concerning SWNCs; the first is about their possible chirality.

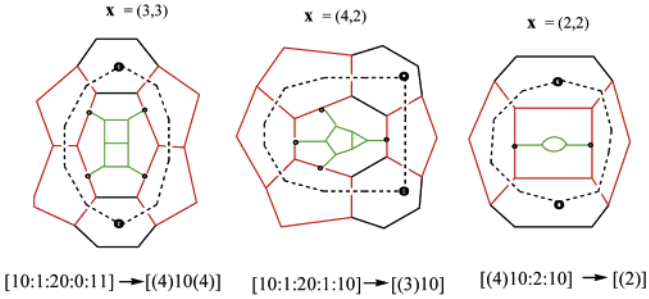

Figure 15. Combinations of smaller polygons derived from four-pentagon buckycones pertaining to both classes 4,1 and 4,2 nanocones. Here, the circumpaths **x** shown are appropriate after the (green) shapes are added.

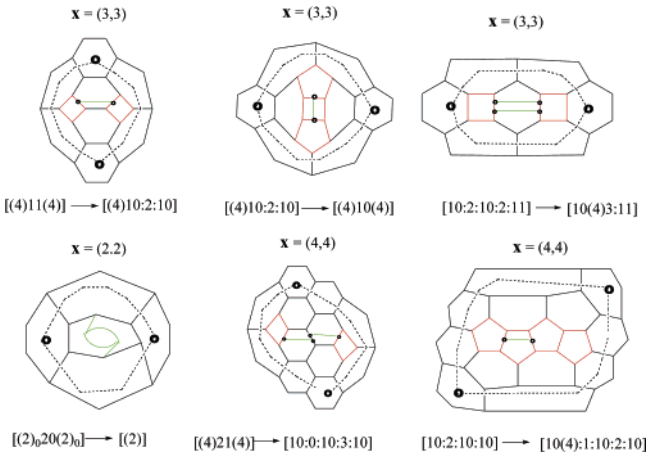

Figure 16. Various apex arrangements for class 4,1 and 4,2 nanocones and associated transformations.

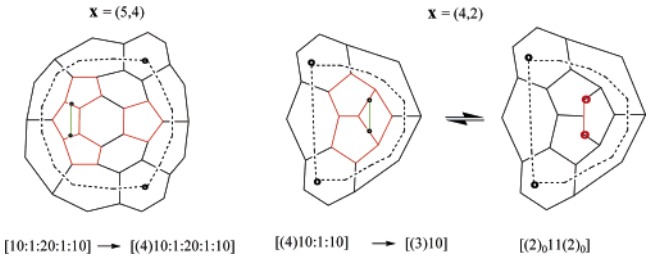

Figure 17. Examples of class 4,1 and 4,2 nanocones and associated transformations.

Indeed, some SWNCs are chiral, whereas others are achiral, noting that chirality is not intrinsically a character of the molecular graph but rather of how it is embedded in space. Generally, for a SWNC drawn on a sheet of paper, its mirror image is represented by the same diagram viewed from the back of the sheet of paper, it being understood (by convention) that the preferred canonical view is from the "outside" of the cone (where its apex region appears convex). This interconversion is, for example, indicated in Figure 25, and it is seen simply by reversing each canonical path code from h_{ij},k_{ij} to k_{ij},h_{ij}, it being understood that, if $k = 0$, then the reversed path $[0,k]$ really is $[k,0]$. Especially for $p = 2$ buckycones $[h,k]$, the criteria for chirality and achirality become clear: such a buckycone is achiral if $h = 0$, $h = k$, or $k = 0$, and otherwise it is chiral. Also of note, a circumpath $\mathbf{x} = (x_1, x_2, ..., x_q)$ becomes $\mathbf{x}^* = (x_q, x_2, ..., x_1)$, and therefore, **x** and **x*** meet the same "criteria" of Table 2. As such, no graphene SWNC class is intrinsically chiral. That is, if a SWNC is chiral, then the chirality is "local", so that, through

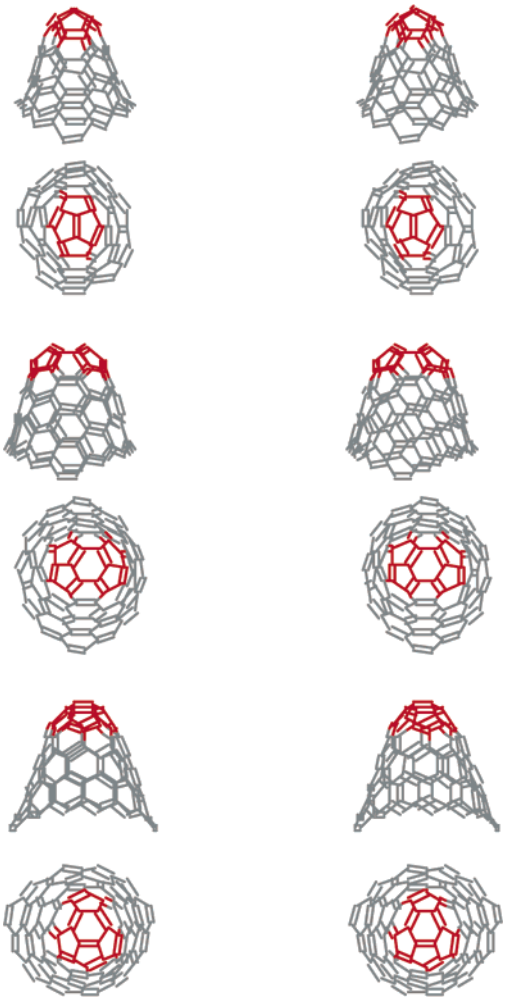

Figure 18. Examples of class 4,1 buckycones: [10:1:10:1:10], [10:1:20:0:11], and [10:1:20:1:10] (top to bottom)

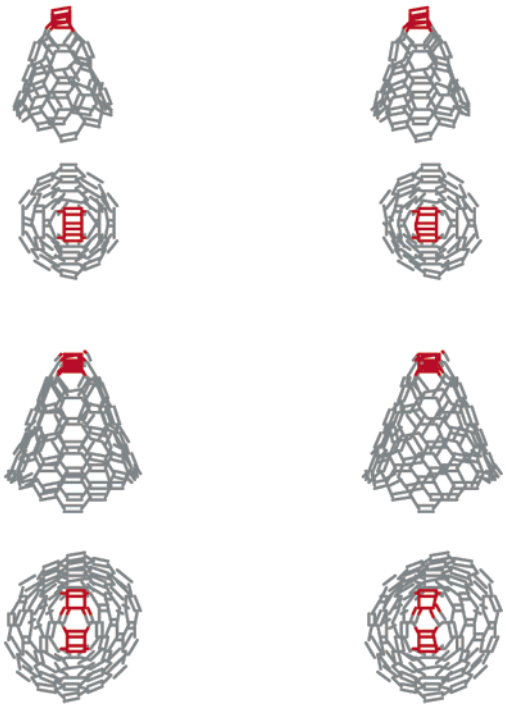

Figure 19. Examples of class 4,1 nanocones with two squares in stereoviews: [(4)10(4)] and [(4)20(4)] (top to bottom).

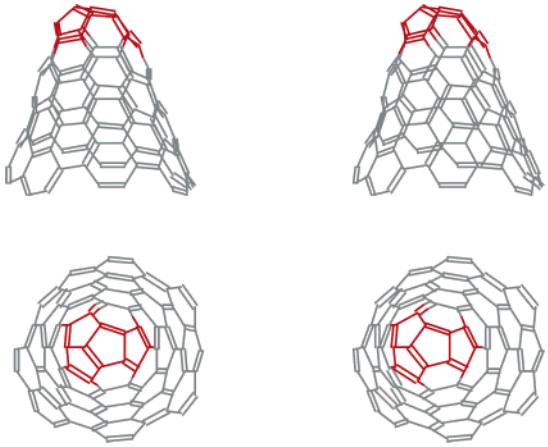

Figure 20. Stereoview of a class 4,2 nanocone [10:1:10:2:10].

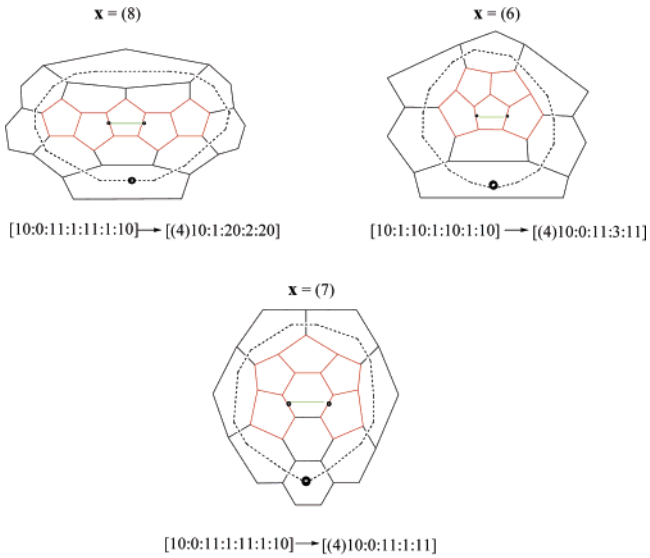

Figure 21. Examples of interconversions between nanocones of class 5,1.

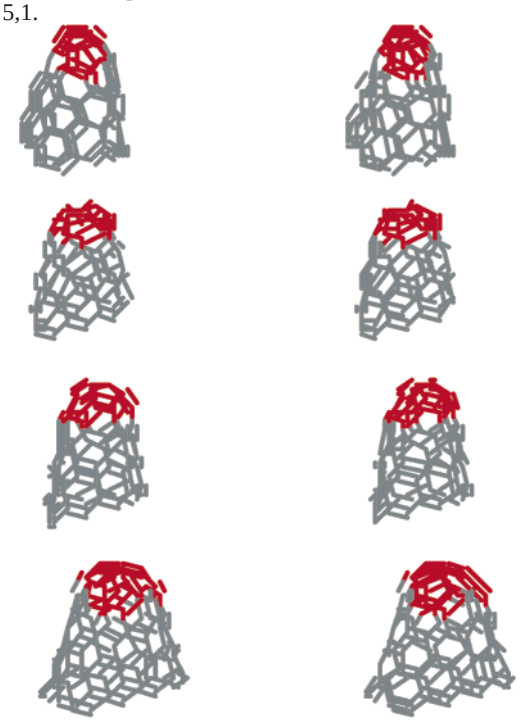

Figure 22. Class 5,1 nanocones with five pentagons in different arrangements (side view); the corresponding front views and codes are shown in Figure 23.

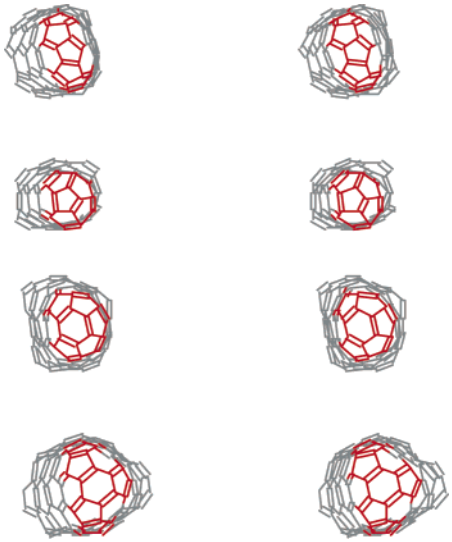

Figure 23. Class 5,1 nanocones from Figure 22 from the front view: [10:0:11:1:11:1:10], [10:1:10:1:10:1:10]. [10:0:11:1:11:1:10], and [10:1:11:1:11:0:21].

a finite sequence of "reactions", it may be changed into its enantiomer.

A second point, which has been an emphasis of this paper, is the provision of a simple means by which to identify a nanocone's class, particularly for disclination numbers (p = 2, 3, 4) where there are two distinct classes. There is the general approach where one identifies a circumpath **x** around the "defect" region and then checks the criteria from Table 2. But, in some cases, we have here found even simpler identifications. We start with cubic nanocones, whence, if there is a single defect ring, one has a straightforward implication:

$$\text{one } p\text{-gon} \Rightarrow \text{class } p,1$$

Stereoviews of three such regular SWNCs (for the two-class disclination numbers p = 2, 3, and 4) appear in Figure 26.

When there are just two defect rings (of size three, four, or five) in a cubic nanocone, a further set of implications also apply:

$$\text{cone } [hk] \Rightarrow \begin{cases} \text{class 2,1 if } |h-k| = 3m \\ \text{class 2,2 if } |h-k| \neq 3m \end{cases}$$

$$\text{cone } [(4)hk] \Rightarrow \begin{cases} \text{class 3,1 if } h \text{ and } k \text{ are both even} \\ \text{class 3,3 if } h \text{ or } k \text{ are odd} \end{cases}$$

$$\text{cone } [(4)hk(4)] \Rightarrow \text{class 4,1}$$

$$\text{cone } [(3)hk] \Rightarrow \begin{cases} \text{class 4,1 if } |h-k| = 3m \\ \text{class 4,2 if } |h-k| \neq 3m \end{cases}$$

For three or more nonhexagonal rings, the procedure via circumpaths is recommended.

These various simplest rules for class identification do not generally cover all cases, if p = 3 or 4, even for the buckycones. But, even the explicitly **x**-dependent criteria of Table 2 are not overly difficult to apply. In general, the defect region need not be a planar network and, indeed, might often be nonplanar if a curved nanocone is somehow seeded by some catalyst nanoparticle in the apical defect region (as often seems the case for the p = 6 nanotubes). In such a general case, one resorts to circumpaths. But, for the planar

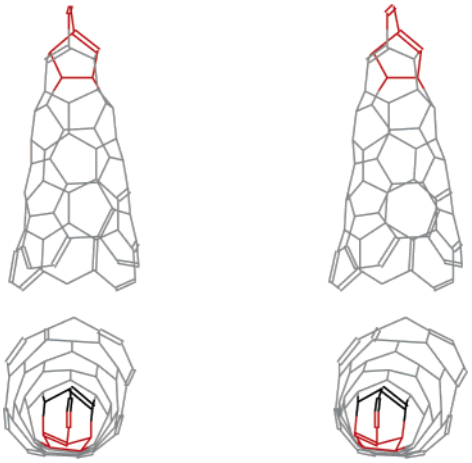

Figure 24. Class 5,1 nanocone [(2)11] with a pentagon and a lune (a C═C double bond) at the apex.

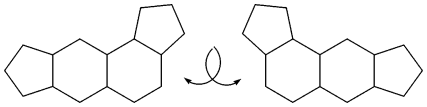

Figure 25. Enantiomeric apex regions of chiral buckycones [21] and [12].

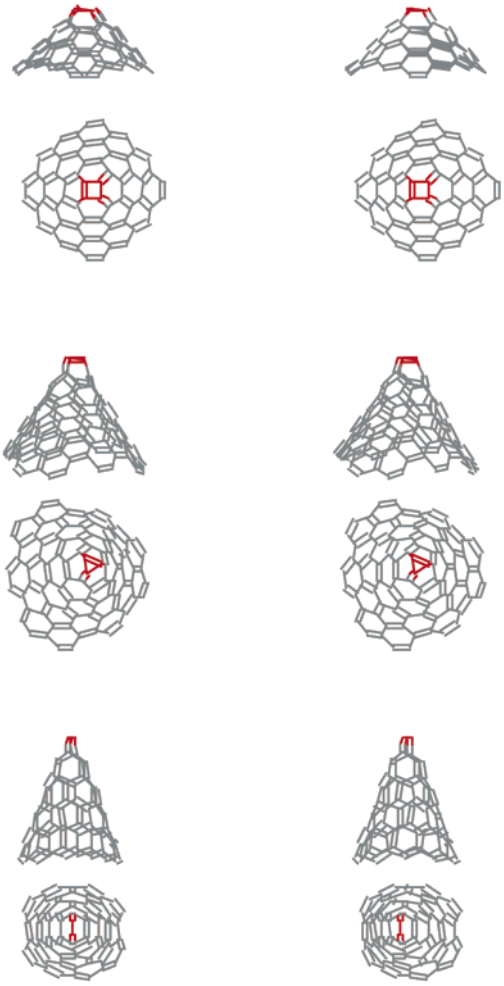

Figure 26. Stereoviews of "regular" nanocones [(p)] for p = 4, 3, and 2. They belong to classes (4,1), (3,1), and (2,1), respectively.

case, there remain a few simplifying remarks which may be added. First, all vertexes of degrees other than 3 may be viewed to be eliminated in some appropriate fashion. The

degree-1 vertexes are simply deleted (along with the incident edge). Next, the degree-2 vertexes are deleted and the consequent dangling pair of bonds connected to leave two smaller polygons. Degree-4 vertexes are split into two degree-3 vertexes (>•< → >•—•<) with the polygons containing the new edge between the two new degree-3 sites each being increased in size by 1. Thence, the special case of cubic nanocones (with all vertexes of degree 3) results.

A third main point of the paper concerns nomenclature for individual nanocones. Again, this is simplest for $p = 1$ and 2, whereafter, for $p = 3$, 4, and 5, the nomenclature increases in complexity, though it all seems to be fairly well in hand for buckycones, and perhaps even for cubic nanocones, with no rings of a size larger than six.

Granted such nomenclature, various derived nanocone invariants can be introduced to characterize the cones. For example, the *diameter* of the apex region of a SWNC can be defined as

$$D_{\text{apex}} = \max_{i,j}(h_{ij} + k_{ij})$$

where i and j identify the different anomalous (defecting) rings. Granted defect rings a and b defining such a diameter, one may choose a ring c within a distance $\lceil D_{\text{apex}}/2 \rceil \equiv r_{\text{apex}}$ of both a and b as a *center* of the apex region, and the set of rings within a (ring-center to ring-center) distance r_{apex} of c is defined as the *apex region*. Then, its *surface area* A_{apex} would be the number of these rings. This surface area should be bounded (for our positive-curvature cones) by the planar value $A_{\text{apex}} \leq \pi r_{\text{apex}}^2$ with the upper bound achieved only if all the defecting is on the outer boundary of this region (so that the inner part looks like undefected graphite). If all of the curvature except that of the two rings at the boundary is done at the center c, then a lower bound is $A_{\text{apex}} \geq \{(q-2)/6\}\pi r_{\text{apex}}^2$ (corresponding to the removal of $q-2$ sectors at c). Evidently then, the quantity

$$s_{\text{apex}} \equiv \frac{\{A_{\text{apex}} - [(q-2)/6]A_{\text{apex}}\}}{\pi r_{\text{apex}}^2} = \frac{A_{\text{apex}}}{3\pi r_{\text{apex}}^2}\{4 - q/2\}$$

is a characteristic of the shape of the apex of the cone; it ranges from ≈0 for the associated Gaussian curvature (and associated defect rings or sites) disparately distributed within the apex region up to ≈1 when the Gaussian curvature occurs at the apex-region boundary. Yet another measure of the size and shape of the apex region is a *Wiener-index analogue*

$$W_{\text{apex}} = \sum_{i<j}(h_{ij} + k_{ij})$$

which increases with p at a fixed shape but also typically increases with p at fixed a D_{apex}. Also, since the h_{ij},k_{ij} paths, when viewed with respect to a regular honeycomb lattice, are typically composed of two noncollinear segments (of lengths h_{ij} and k_{ij}), one might entertain the use of "geometric" distances. That is, $h_{ij} + k_{ij}$ in the above formulas would be replaced by $\{h_{ij}^2 + h_{ij}k_{ij} + k_{ij}^2\}^{1/2}$.

Finally, there is a point related to the simple class-identification criterion for $p = 2$ buckycones. As shown in Appendix B, these buckycones [hk] fall into class 2,1 or 2,2 as $|h - k|$ is or is not divisible by 3. And, as explicated in Appendix D, this is intriguingly related to other situations: first, to stability criteria for icosahedral-symmetry fullerenes; second, to 0-band gap criteria for the delocalized bond orbitals of nanotubes; and third, to Clar-sextet positioning in graphite. Further, a suggestion arises (in Appendix D) that the class-2,2 buckycones might generally accumulate more molecular orbital (or band) levels near the Fermi level than those of class 2,1.

CONCLUSIONS

Eight different classes of positive-curvature graphitic nanocones have been described, characterized, and illustrated. It is emphasized that each class is as distinct from one another as each is from graphite, insofar as concerns the "ease" of changing from one to the other. Unique codes have been given for the buckycones and for a large collection of nanocones with ring sizes other than five and six or with vertex degrees other than 3. Illustrations of few-atom (few-bond) transformations among nanocones within each of the eight classes have been given, it being emphasized that, for an overall "radius" R nanocone, any transformation between classes is nonlocal in entailing breaking and making $\sim R$ bonds (regardless of whether the classes have the same curvature or not). Simple means by which to identify nanocones with classes have been established, including the further cases of negative-curvature cones. Meaningful size measurements of nanocone apex regions have been suggested.

There still are several questions. For general nanocones at $p = 3$ and 4 disclinations, simpler class-identification criteria (without explicit reference to circumpaths) might be desired. One might inquire as to the relative stabilities of different local structures within each class. To similarly compare between classes is a more delicate matter, as there might be class-specific electronic structural features, some hint of such for classes 2,1 and 2,2 appearing in Appendix D. Since radius-R nanocones might be viewed as graphite with $\sim R$ local defects, one might anticipate the possibility of up to $\sim R$ notably displaced molecular orbital levels, and particularly, the question arises as to whether they might be displaced or near to the Fermi level. Though one might surmise such a particular type of displacement to be unlikely, this has been found[21] to occur rather frequently with R-defected graphite where the R local defects correspond to cutting a boundary of length $\sim R$. Of course, from class-specific electronic-structure features, there should follow class-specific properties, potentially manifesting more dramatic differences than for cones within the same class. Thus, several interesting general problems remain for future work.

ACKNOWLEDGMENT

Acknowledgment is made to the Welch Foundation of Houston, Texas (through Grant BD-0894).

APPENDIX A. CLASSIFICATION CRITERIA

It is of interest to prove the simply implementable classification criteria in the last column of Table 2 (and paralleling the simple square-lattice criteria in ref 20). In ref 19, the classification criteria were more complexly expressed: given a circumpath $\mathbf{x} \equiv (x_1, x_2, ..., x_q)$, apply to the different (initiating) vectors $\mathbf{m} \equiv (m_1, m_2, ..., m_q)$ at the

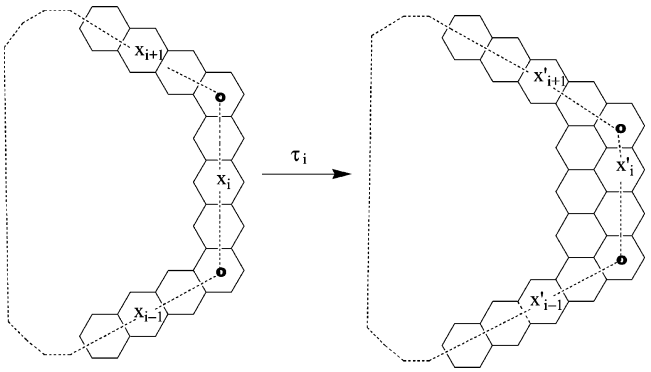

Figure 27. Transformation of a circumpath by a single step extension outward at an acenic strip (of length ≥ 2).

given q the "expansion" transformations τ_i, while possibly also cyclically permuting the **x** components to see which **m** can yield **x**. Here, the *expansion transformations* τ_i act on a general circumpath **x** to change the components of **x** thusly:

$$x_1 \rightarrow x_1 + 1, \qquad q = 1$$

$$x_j \rightarrow \begin{Bmatrix} x_i - 1, & j = i \\ x_j + 2, & j \neq i \end{Bmatrix}, \qquad q = 2$$

$$x_j \rightarrow \begin{Bmatrix} x_i - 1, & j = i \\ x_j + 1, & j = i \pm 1 \\ x_j, & \text{otherwise} \end{Bmatrix}, \qquad q \geq 3$$

where the subscripts are taken modulo q (i.e., $x_{q+1} = x_1$ and $x_0 = x_q$). This transformation τ_i corresponds to the expansion of a circumpath $\mathbf{x} \equiv (x_1, x_2, ..., x_q)$ out one step farther along the ith side (x_i) of **x** to give $\mathbf{x}' = \tau_i\mathbf{x}$, as indicated in Figure 27. The cyclic permutation transformation C carries **x** to $\mathbf{x}' = C\mathbf{x}$ with $x'_i = x_{i-1}$. Alternatively, one can start with **x** and apply inverses τ_i^{-1} along with permutations C, to ultimately obtain one of the canonical **m** labels. Anyway, granted this previous class characterization, we now wish to establish the more readily checkable characterization of the last column of Table 2.

First, the cases with $q = 1$ and $q = 5$ are trivial since there is but one class at each q. Indeed, the cases $q = 6k \pm 1$, with $k \geq 1$, are similarly trivial.

For $q = 2$, we simply check to see that, for τ_1,

$$x'_2 - x'_1 = (x_2 + 2) - (x_1 - 1) = (x_2 - x_1) + 3$$

so that τ_1 conserves the 3 divisibility of the difference of the components of $\mathbf{x} = (x_1, x_2)$. Clearly, the same applies to the other transformations τ_2 and (the cyclic permutation) C. At the same time, one sees that the two initiating vectors **m** $= (0,0) \equiv \mathbf{0}$ and $\mathbf{m} = (0,1) \equiv \mathbf{e}_2$ have different 3 divisibilities of the component differences (respectively, 0 and 1), so that the two different classes are neatly identified. (The value of the particular remainder of 1 or 2 when a difference is not divisible by 3 is not generally conserved since C interchanges these remainders.)

For $q = 3$, the application of an expansion transformation τ_i to a circumpath **x** clearly changes the parity of each component x_i and, thence, the mod-2 values of each x_i by 1. Thus, the multisets of mod-2 values of the components of **x** are changed in accordance with one of the pattern interchanges

$$\{0,0,0\} \leftrightarrow \{1,1,1\} \text{ or } \{0,0,1\} \leftrightarrow \{1,1,0\}$$

Evidently, the sums

$$(x'_1)_{\text{mod}-3} + (x'_2)_{\text{mod}-2} + (x'_3)_{\text{mod}-2} \text{ and}$$
$$(x_1)_{\text{mod}-3} + (x_2)_{\text{mod}-2} + (x_3)_{\text{mod}-2}$$

have the same 3 divisibility. Clearly, the same is also true for C. And, at the same time, the two initiating-vector labels **m** $= (0,0,0) \equiv \mathbf{0}$ and **m** $= (0,0,1) \equiv \mathbf{e}_3$ have different 3 divisibilities for the sums of the modulo-2 components. Further, more generally, when we apply τ_i to obtain $\mathbf{x}' = \tau_i\mathbf{x}$, one finds

$$\sum_{j=1}^{q}(x'_j)_{\text{mod}-2} = \sum_{j=1}^{q}(x_j)_{\text{mod}-2} + \Delta[\text{mod}_2(x_{i-1})_{\text{mod}-2} + (x_i)_{\text{mod}-2} + (x_{i+1})_{\text{mod}-2}]$$

Then, via the same argument already mustered, one finds that the 3 divisibility of the mod-2 sum of the components of a circumpath **x** is conserved under the expansion transformations (and, even more clearly, that of the cyclic permutations). Generally, then, the 3 divisibility of this sum distinguishes the pairs of classes at $q = 6k + 3$ (k being a nonnegative integer) with **m** vectors **0** and $\mathbf{e}_q$.

For the case of $q = 4$, the proof rather closely follows that for $q = 2$. That is, one readily finds

$$x'_2 + x'_4 - (x'_1 + x'_3) = x_2 + x_4 - (x_1 + x_3) \pm 3$$

so that the 3 divisibility of this difference of **x** components is conserved. Indeed, a similar result follows rather closely for $q = 6k \pm 2$, where $k \geq 1$. The same sort of result, in fact, applies for $q = 6$, though in this case, much more is conserved, namely, the Burgers defect vectors, for example, as described in ref 19.

Thus, the criteria of the last column of Table 2 are established, as well as analogous results for the negative-curvature cones with $q \geq 7$. These correct the announced (but unproved) criteria of ref 20 for graphitic cones. The corresponding simple criteria of ref 20 for the classification for cones from the square-planar lattice are, however, correct (as there established).

APPENDIX B. CLASSES (2,1) AND (2,2) OF 2-DISCLINATION BUCKYCONES

The direct relation between the relative positions of $p = 2$ pentagons and the class designation of $(p,\mathcal{M}) = (2,1)$ or (2,2) is to be established. At the same time, we note that, when cutting out multiple 60° sectors from a graphene sheet to generate a nanocone, the sectors need not be contiguous. In particular, to generate a 2-disclination buckycone [hk], simply remove a sector from each of two hexagons at a relative position h, k to one another, as indicated in Figure 28. There, in addition to the two consequent pentagons (resulting on the joining of dangling bonds on opposite edges of the deleted sectors), we indicate a circumpath $\mathbf{x} = (x_1, x_2, x_3, x_4)$. The integer number

$$\text{mod}_2(x_1) - \text{mod}_2(x_2) + \text{mod}_2(x_3) - \text{mod}_2(x_4) = 2[\text{mod}_2(h) - \text{mod}_2(k)]$$

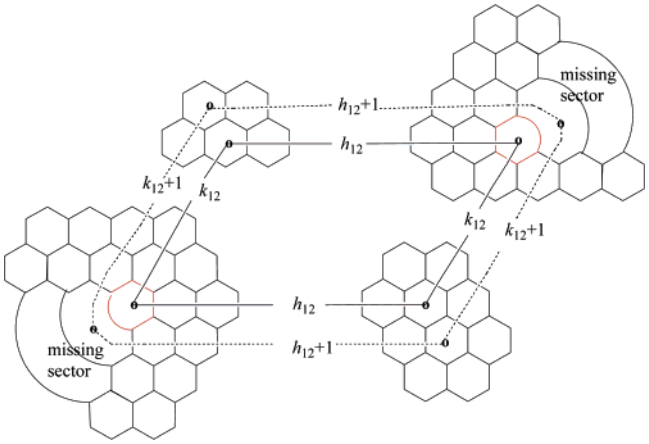

Figure 28. A 2-disclination buckycone apex with two pentagons (red) coded by $[h_{12}k_{12}]$ having a circumpath $\mathbf{x} = (h_{12} + 1, k_{12} + 1, h_{12} + 1, k_{12} + 1)$.

is seen to be divisible by 3, depending on whether h and k are of the same parity or not. That is, if h and k for a $p = 2$ buckycone are of the same parity, then the cone falls in class $(p,\mathcal{M}) = (2,1)$, and otherwise, it is in class $(p,\mathcal{M}) = (2,2)$.

APPENDIX C. CUBIC NANOCONES WITH TWO DEFECT RINGS

Simple criteria for class designation are readily established so long as we have a cubic nanocone with just two nonhexagonal rings. That is, the criteria are simply in terms of the canonical path h, k between the two rings, with the proof proceeding much as that for the $p = 2$ buckycones in Appendix B. First, for $p = 3$, consider a square and a pentagon separated by an h, k path, whence a construction much as in Figure 28 applies but now with two adjacent 60° sectors deleted in the lower left. As a consequence, the outer counterclockwise path from ring **a** to ring **b** (around the incipient square in the lower left) is acenic, and we have identified a circumpath $\mathbf{x} = (x_1, x_2, x_3)$ with $x_1 = h + k + 1$, $x_2 = h + 1$, and $x_3 = k + 1$. Then, the cone falls into class 3,1 if the criteria number

$$\mathrm{mod}_2(x_1) + \mathrm{mod}_2(x_2) + \mathrm{mod}_2(x_3) = \mathrm{mod}_2(h + k) + \mathrm{mod}_2(h) + \mathrm{mod}_2(k)$$

is divisible by 3, and otherwise, it falls into class 3,3. But, as the $[h,k]$ parities are [0,0], [0,1], [1,0], or [1,1], this number takes the respective values 0, 2, 2, or 2. Thus, the nanocone is class 3,1 if both h and k are even, and otherwise, it is class 3,3.

The $p = 4$ case with two squares is rather similarly treatable. Two sectors are deleted at both the lower left and upper right in Figure 28, whence there results a circumpath $\mathbf{x} = (x_1, x_2) = (h + k + 1, h + k + 1)$. Thence, the criteria number $|x_1 - x_2| = 0$, and the nanocone is necessarily of class 4,1.

The $p = 4$ case with a triangle and a pentagon requires a little more development. Here, we delete three sectors from the lower left (incipient triangle) ring while just one sector is deleted at the upper right, as shown in Figure 29. There, for $h > k$, a circumpath $\mathbf{x} = (x_1, x_2)$ is identified, with $x_1 = 2k + 1$ and $x_2 = h + k + 1 + h - k$, so that the criteria numberis divisible by 3, in correspondence with the 3

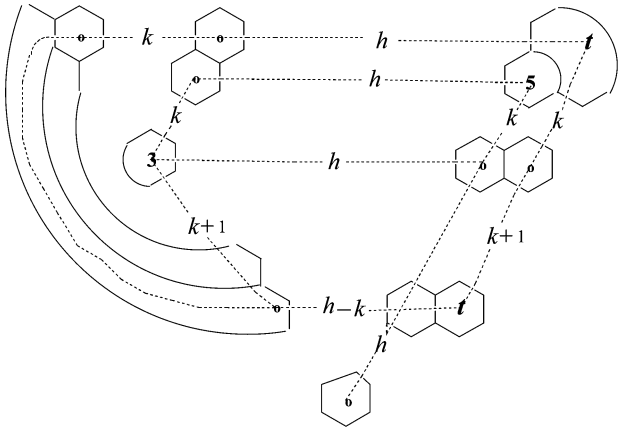

Figure 29. The designation of a circumpath around the triangle−pentagon defect region, with the triangle and pentagon marked by **3** and **5**, respectively. The circumpath starts from the hexagon marked with a ***t*** in the upper right and proceeds (counterclockwise) along the dotted line through the hexagons marked either with an **o** (where is no turn) or with a ***t*** (where there is a turn).

$$x_2 - x_1 = 2(h - k)$$

divisibility of $h - k$. A similar result is found for $h = k$ and (by symmetry) for $h < k$. Thus, such a nanocone is in class 4,1 if $h - k$ is divisible by 3, and otherwise, it is in class 4,2.

APPENDIX D. INTER-RELATIONS INVOLVING CANONICAL PATHS

The canonical path label $[h,k]$, in addition to neatly identifying classes for 2-disclination buckycones, also makes intriguing related appearances in other contexts. First, such a canonical path $[h,k]$ may be used[21−24] to identify the separation between nearest-neighbor pairs of pentagons in an icosahedral-symmetry fullerene (or buckyball). It then turns out that the 3 divisibility of $h - k$ identifies whether the fullerene is[24] a "leapfrog" fullerene ($h = k + 3m$) or not ($h \neq k + 3m$) and also whether the fullerene is[25] closed-shell ($h = k + 3m$) or open-shell ($h \neq k + 3m$). Yet, further, $h - k$ being divisible by 3 guarantees[25] a Kekulé structure with all double bonds (favorably) occurring in hexagons.

Second, such a canonical path designation appears in the classification[26] of buckytubes, with the path $[h,k]$ being such that the initial and final hexagons coincide (or, equivalently, if acenic paths at 120° to one another are found to intersect down the tube at distances h and k along the two acenic paths). Here (within the approximation of the simple Hückel model), the band-gap Δ of an (infinite) buckytube depends[26] simply on the 3 divisibility of $h - k$. That is, $\Delta = 0 \Leftrightarrow h = k + 3m$.

Third, such canonical paths designate separations between Clar sextets in graphite (or other fully benzenoid species). That is, if a graphene sheet is marked with Clar sextet circles, being[26] disjointed hexagons, such as to cover all sites, then it is easy to see that the different Clar sextets are separated by $[h,k]$ paths with $h - k$ divisible by 3 (within a single overall Clar structure with a maximum number of Clar sextets).

Evidently, as seen from the Clar-sextet coincidence, all class 2,1 nanocones [*hk*] may be viewed to have pentagons replacing two "sextet" hexagons on the surviving four sectors of such a Clar-sextet-labeled graphene sheet, whereas all class 2,2 nanocones [*hk*] have one pentagon replacing a "sextet" hexagon and the second pentagon replacing a "nonsextet" hexagon. But, from the coincidence for icosahedral-symmetry fullerenes, the occurrence of pentagons at separations of [*h*,*k*] with $h - k$ divisible by 3 seems to impart a special stability (and nonzero HOMO−LUMO gap). Thence, this seems to suggest that the class 2,2 nanocones have a greater extent of piling up of molecular orbital levels at the Fermi level (or HOMO/LUMO level), as compared to the class 2,1 nanocones.

REFERENCES AND NOTES

(1) Balaban, A. T.; Klein, D. J.; Liu, X. Graphitic cones. *Carbon* **1994**, *32*, 357−359.

(2) Balaban, A. T. Theoretical investigations of single-wall nanocones. In *Nanostructures. Novel Architecture*; Diudea, M. V., Ed.; Nova Publishers: New York, 2005; pp 113−142.

(3) Ebbesen, T. W. Cones and tubes: Geometry in the chemistry of carbon. *Acc. Chem. Res.* **1998**, *31*, 558−566.

(4) Burgers, J. M. Some considerations on the fields of stress connected with dislocations in a regular crystal lattice. I and II. *Proc. K. Ned. Akad. Wet.* **1939**, *42*, 293−325; 378−399.

(5) Read, R. T. *Dislocations in Crystals*; McGraw-Hill: New York, 1953.

(6) Cotrell, A. H. *Theory of Crystal Dislocation*; Blackie & Son: London, 1964.

(7) Sadoc, J. F.; Mosseri, R. *Geometrical Frustration*; Cambridge University Press: New York, 1999.

(8) Klein, D. J.; Liu, X. Elemental carbon isomerism. *Int. J. Quantum Chem.* **1994**, *28*, 501−523.

(9) Klein, D. J. Topo-graphs, embedding and molecular structure. In *Chemical Topology*; Bonchev, D., Rouvray, D. H., Eds.; Gordon and Breach: Amsterdam, The Netherlands, 1999; pp 39−83.

(10) Gillot, J.; Bollmann, W.; Lux, B. Cristaux de graphite en forme de cigare et à structure conique. *Carbon* **1968**, *6*, 381−387.

(11) Haanstra, H. B.; Knippenberg, W. F.; Verspui, G. Columnar growth of carbon *J. Cryst. Growth* **1972**, *16*, 71−79.

(12) Double, D. D.; Hellawell, A. Cone-helix growth forms of graphite. *Acta Metallurg.* **1974**, *22*, 481−487.

(13) Krajnovich, D. J.; Vasquez, J. E.; Savoy, R. J. Impurity-driven cone formation during laser sputtering of graphite. *Science* **1993**, *259*, 1590−1592.

(14) Ge, M.; Sattler, K. Observation of fullerene cones. *Chem. Phys. Lett.* **1994**, *220*, 192−196.

(15) Sattler, K. Scanning tunneling microscopy of carbon nanotubes and nanocones. *Carbon* **1995**, *33*, 915−920.

(16) Sattler, K. Growth and scanning probe microscopy of buckytubes and buckycones. *Surf. Rev. Lett.* **1996**, *3*, 813−818.

(17) Han, J.; Jaffe, R. Energetics and geometries of carbon nanoconic tips. *J. Chem. Phys.* **1998**, *108*, 2817−2823.

(18) Murata, K.; Kaneko, K.; Steele, W. A.; Kokai, F.; Takahashi, K.; Kasuya, D.; Hirahara, K.; Yuduasaka, M.; Ijima, S. Molecular potential structures of heat-treated single-wall carbon nanohorn assemblies. *J. Phys. Chem. B* **2001**, *105*, 10210−10216.

(19) Klein, D. J. Topo-combinatoric categorization of quasi-local graphitic defects. *Phys. Chem. Chem. Phys.* **2002**, *4*, 2099−2110.

(20) Klein, D. J. Quasi-local defects in regular planar networks: categorization for molecular cones. *Int. J. Quantum Chem.* **2003**, *95*, 600−616.

(21) Klein, D. J.; Bytautas, L. Unpaired π-electron spins *J. Phys. Chem.* **1999**, *103*, 5196−5210.

(22) Goldberg, M. A class of multi-symmetric polyhedra. *Tohoku Math. J.* **1937**, 104−108.

(23) Coxeter, S. M. Virus macromolecules and geodesic domes. In *A Spectrum of Mathematics*. Butcher, J. C., Ed.; Auckland University Press/Oxford University Press: New York, 1971; pp 98−107.

(24) Klein, D. J.; Seitz, W. A.; Schmalz, T. G. Icosahedral-symmetry carbon cages. *Nature* **1986** *323*, 703−706.

(25) Fowler, P. W. How unusual is C_{60}: Magic numbers for carbon clusters. *Chem Phys. Lett.* **1986**, *131*, 444−450.

(26) Fowler, P. W.; Steer, J. I. The leapfrog principle: A rule for electron counts of carbon clusters. *J. Chem. Soc., Chem. Commun.* **1987**, 1403−1405.

(27) Fowler, P. W. Localized models and leapfrog structures of fullerenes. *J. Chem. Soc., Perkin Trans. 2* **1992**, 145−146.

(28) Klein, D. J.; Seitz, W. A.; Schmalz, T. G. Symmetry of infinite tubular polymers: Application to buckytubes. *J. Phys. Chem.* **1993**, *97*, 1231−1236.

CI0503356